J Mater Sci (2008) 43:5626–5633
DOI 10.1007/s10853-008-2721-z

Studies on the crystallization process of BEA/MOR co-crystalline zeolite

Xiaolan Qi · Dejin Kong · Xiaohong Yuan · Zhongqiang Xu · Yangdong Wang · Junlin Zheng · Zaiku Xie

Received: 7 January 2008 / Accepted: 12 May 2008 / Published online: 18 July 2008

Abstract BEA/MOR co-crystalline zeolite was synthesized using tetraethylammonium-fluorides as composite templates. The crystallization process of BEA/MOR co-crystalline zeolite was systematically investigated based on XRD, ICP, SEM, TGA, and nitrogen adsorption characterizations. Through the XRD patterns of the samples with different crystallization times, the BEA and MOR phases did not appear simultaneously in the crystallization process. The BEA phase was the favored product at the beginning of crystallization, whereafter the MOR phase emerged, and the BEA/MOR co-crystalline zeolite was gradually formed. The morphology of obtained particles changed a little during the crystallization process, but the granularity distribution range broadened. Asymmetry of BEA/MOR co-crystalline zeolite particles led to uneven distribution of the mesopores. It is showed that the pore size distribution of the samples with more than 90-h crystallization period exhibited bimodal mesopores distribution, and the pore sizes of the extra mesopores were 4.9 and 5.6 nm, respectively. Based on these results, the crystallization mechanism of BEA/MOR co-crystalline zeolite in tetraethylammonium-fluoride binary templates was roughly proposed.

X. Qi (✉) · D. Kong · X. Yuan · Z. Xu · Y. Wang · J. Zheng · Z. Xie
Shanghai Research Institute of Petrochemical Technology, SINOPEC, 1658 Pudong Beilu, Shanghai 201208, People's Republic of China
e-mail: qixl@sript.com.cn

J. Zheng
e-mail: zjl@sript.com.cn

Z. Xie (✉)
e-mail: xzk@sript.com.cn

Introduction

Zeolites, such as Y, ZSM-5, mordenite and zeolite beta, possess several catalytically desirable properties, such as high-surface area, abundant uniform microporous structures with adjustable pore size, acidity and high stability. These phase-pure microporous zeolites are widely used as acid catalysts in a diversity of commercial processes, especially in the petrochemical industry. In fact, perfect crystalline phases do not exist strictly. The majority of zeolite crystallization conditions used result in the formation of co-crystalline zeolite or intergrowth materials. However, the catalytic performance of co-crystalline zeolite materials aroused little interest for a long time, because co-crystalline zeolite materials were usually regarded as hybrid crystals [1–5].

As a kind of extended defects, intergrowth have frequently been observed in zeolites crystallization and well documented in several families of microporous materials [6]. Rao and Thomas [7] proposed an overview of different types of intergrowths relevant to zeolites in which intergrowths were classified into two types: polytypism and epitaxy or overgrowth. Polytypism arises when distinct layers are stacked according to a specific sequence, and overgrowth occurs when one crystalline phase grows on the face of another phase. Two zeolite topologies which can form intergrowth should be structurally related or have the same planar building units. The structural similarities enable the intergrowth between such zeolite frameworks under specific synthesis conditions. For instance, MFI/MEL intergrowth material has often been reported [6, 8] because topologically related frameworks can be built from the same building blocks, but in different arrangement. Common intergrowths formed in zeolites include MFI/MEL, FAU/EMT [9–11], MAZ/MOR (ECR-1) [6, 12], ERI/OFF [6, 13–15], BEA/MOR [1, 16], STF/SFF [17] and so on (the three-letter codes

referring to specific structure types [18]). Usually, intergrowth takes place on a specific crystal face. Polytypical intergrowths are often realized by a one-step synthesis, but overgrowth is usually obtained by two-step synthesis [10, 19, 20]. These core–shell type composite zeolites could be used for changing crystal surface properties.

The BEA and MOR zeolite topologies with similar 12-membered ring channels are structurally related, and TEAOH (tetraethylammonium hydroxide) or TEABr (tetraethylammonium bromide) were usually used as structure-directing agent of both BEA and high-silica MOR zeolites, which brought the possibility of their co-crystalline composites under specific synthesis conditions. The synthesis of zeolites in alkaline media with fluoride anions has some special character. For instance, fluoride anions play the structure-directing agent role and contribute to the stable effect on siliceous mordenite [21, 22], and the acidity strength of H-BEA zeolites was increased [23]. Considering the role fluoride anions played, we designedly synthesized BEA/MOR co-crystalline zeolite by using tetraethylammonium-fluoride as the binary templates and silica sol as the silica source, respectively [16]. The physicochemical properties of BEA/MOR co-crystalline zeolite were significantly different from that of the mechanical mixtures of corresponding composites [1, 24]. Recently, it was found that BEA/MOR co-crystalline zeolite had much higher acid strength than their mechanical mixtures when mordenite phase content exceeds 50%. The BEA/MOR co-crystalline zeolite with 65% mordenite phase content showed the highest acid strength exceeding mordenite or zeolite beta [1, 24]. Furthermore, the catalytic activity on methanol dehydration to produce dimethylether over BEA/MOR exhibits a volcano-type curve in which the methanol conversion increases with increasing mordenite phase content to a maximum and then decreases. This is in good agreement with its change trend of strong acid intensity. Besides high catalytic activity, BEA/MOR also showed high stability as a result of reducing deactivation tendency due to coke formation [1].

Close relationship exists between the macroscopic properties and the microscopic structure of zeolites. In the present work, the crystallization process of the BEA/MOR co-crystalline zeolite were systematically investigated through the XRD, SEM, ICP, TGA, and nitrogen adsorption characterizations, and the crystallization mechanism of BEA/MOR co-crystalline zeolite in tetraethylammonium-fluoride binary templates was roughly proposed.

Experimental

Synthesis

The sodium form of zeolite was synthesized hydrothermally under the static conditions according to our previous work [16] using the batch composition:

$1Al_2O_3 \bullet 25SiO_2 \bullet 6.25TEAOH \bullet 2.5F$

The typical synthesis procedure was as follows: (1) 10.7 g of sodium fluoride (AR, 98%, Sinopharm Chemical Reagent Co., Ltd.) was added into 365.2 g TEAOH (Industrial product, 25% aqueous solution, Hangzhou Greenda Chemical Co., Ltd.) solution in a 1,000 mL beaker and stirred until NaF was dissolved completely at room temperature; (2) 24.9 g sodium aluminate (CP, >41% Al_2O_3, Sinopharm Chemical Reagent Co., Ltd.) was added to this solution under vigorous stirring; (3) 375 g silica sol (Industrial product, 40% SiO_2, Jiangyin Xiagang Chemical Plant) was added slowly to the mixture prepared above under stirring; (4) After additional stirring for about 60 min the gel mixture was loaded into PTFE-lined stainless steel autoclaves and heated at 178 °C under autogenous pressure. (5) After the different predetermined crystallization times in the range of 0–100 h, the autoclaves were taken out respectively from the oven to finish the crystallization process. The resulted solid products were recovered by filtration, washed with distilled water and dried in air at 120 °C.

The NH_4-form of samples was obtained by repeated ion exchange with 1 M NH_4NO_3 solution for 2 h at 363 K. The protonated form was then obtained by calcining the NH_4-form at 813 K for 4 h.

Characterization

The powder XRD patterns were recorded on a X-ray powder diffractometer (Bruker D8) using nickel-filtered Cu Kα radiation over 2θ angles ranging from 5 to 50° with scanning step 0.02° and step time 0.01 s. The operating tube voltage and the current were 40 kV and 100 mA, respectively.

After coating with a thin layer of gold, the morphologies of the prepared samples were observed using a Philips XL30 FEG SEM equipped with an EDAX energy dispersive X-ray spectrometer (EDS) (Oxford ISIS-Energy).

TG analysis was performed on a TA4000 thermal analyzer in air at a heating rate of 10 °Cmin^{-1}.

N_2 adsorption–desorption isotherms were obtained at 77 K on a Micromeritics Tristar-3000 apparatus. Samples were degassed for 4 h under vacuum at 350 °C prior to analysis. The specific surface area was calculated using the BET method. The total pore volume was obtained by converting the amount adsorbed at a relative pressure of 0.995 to the volume of liquid nitrogen. The microporous surface area and volume was determined by the t-plot analysis of the adsorption branch of the isotherm. The pore size distributions of samples were analyzed from the desorption branch of the isotherm by the BJH method.

The elemental analysis of the solid samples was performed using inductively coupled plasma apparatus

(P-4010/ICP-AES). The standard deviation of the measurement is less than 5% and the recovery is 98–105%. Three repeats were used in every measurement.

Results and discussion

XRD

The XRD patterns of the samples, which are obtained for the different crystallization time, were showed in Fig. 1. In initial gel, there was no crystalline materials found except a weak diffraction peak at $2\theta = 37.5°$, assigned to part of undissolved NaF [25]. At the beginning of the crystallization, only pure zeolite beta was obtained in solid phase after 20 and 40 h crystallization. The crystallinity of pure zeolite beta increased with the increase of crystallization time. The results showed that the BEA phase was the favored product at the beginning of the crystallization process. After 50 h crystallization, a little mordenite phase was detected besides zeolite beta. After emergence of MOR, the intensity of diffraction peaks corresponding to mordenite phase increased continuously as crystallization process was prolonged. The MOR content was increasing in the sample. Meanwhile, the intensity of diffraction peak at $2\theta = 7.8°$ corresponding to BEA phase was almost invariable before 76 h crystallization, and then decreased in a certain extent. It indicated that the crystallization of zeolite beta was not finished completely.

The intensity of diffraction peak corresponding BEA phase did not decrease obviously until the end of crystallization. Zeolite beta and mordenite were obtained simultaneously during that period and the BEA/MOR co-crystalline zeolite was gradually formed. The decrease of diffraction intensity at the latter of crystallization should be attributed to the decrease of BEA relative content in the co-crystalline zeolite sample. It was different from the crystallization of overgrowth type zeolite. In the case of MOR/MFI type of core-shell composite zeolite, the core material was completely wrapped by an intergrown layer of other zeolite type [19]. These results were also different from Xu and co-workers' results in synthesis of MCM-22/ZSM-35 [2]. They found that the formation of pure MCM-22 and ZSM-35 phases occurred at crystallization time of 60 and 120 h, respectively, while crystallization period from 60 to 120 h led to MCM-22/ZSM-35 composites. The fractions of different phases were not able to be quantified.

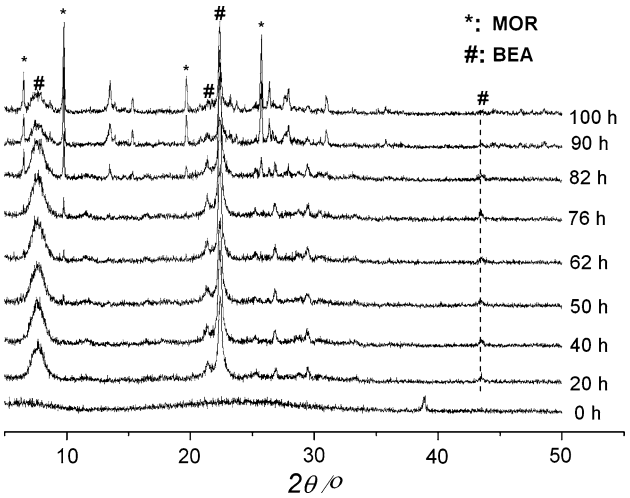

Fig. 1 The XRD patterns of samples obtained during the crystallization process

The framework density of BEA is lower than MOR. The framework density of MCM-22 with MWW [18] topology structure is 15.9 T/nm^3 (T stands for Si or Al), but ZSM-35's with FER [18] topology structure is 17.6 T/nm^3. It can be concluded that zeolite phase with relative open framework structure almost appeared first, and then the other zeolite phases with relative high framework density were generated as a function of crystallization time while synthesizing co-crystalline or intergrowth zeolite. In fact, in our experiment focusing on the phase selection of BEA/MFI intergrowth, the results (not shown in this paper) showed that the BEA was generated first at the same way.

It was estimated that the particles sizes were between 6.9 and 8.3 nm and showed no trends based on X-ray line broadening and the Scherrer equation.

There are several parameters that can affect the phase selection of intergrowth [2, 24, 26]. By adjusting crystallization time, the phase ratio of zeolite beta to mordenite in BEA/MOR co-crystalline zeolite can be controlled in a large range.

SEM

Figure 2 shows SEM micrographs of the five samples at the different crystallization periods. The morphology of the samples evolved during the synthesis process. As shown in Fig. 2a, the initial gel presented amorphous aggregates, its rough surface was high vesicular. After 40 h crystallization (Fig. 2b), the zeolite beta was crystallized as tiny spherical crystals with average size about 50 nm, which were assembled to nearly monodisperse large ellipsoidal particles with average size of 0.6 μm. While crystallization time was elongated to 76 h, the size of a few particles became larger as the mordenite phase appeared and its content increased (Fig. 2c). As the crystallization time was further increased to 90–100 h, the morphology of the aggregates particles was not changed obviously (Fig. 2d–e). The granularity distribution range was broadened, but average size was lower than general pure mordenite evidently. Individual sheet-like crystals could be found occasionally

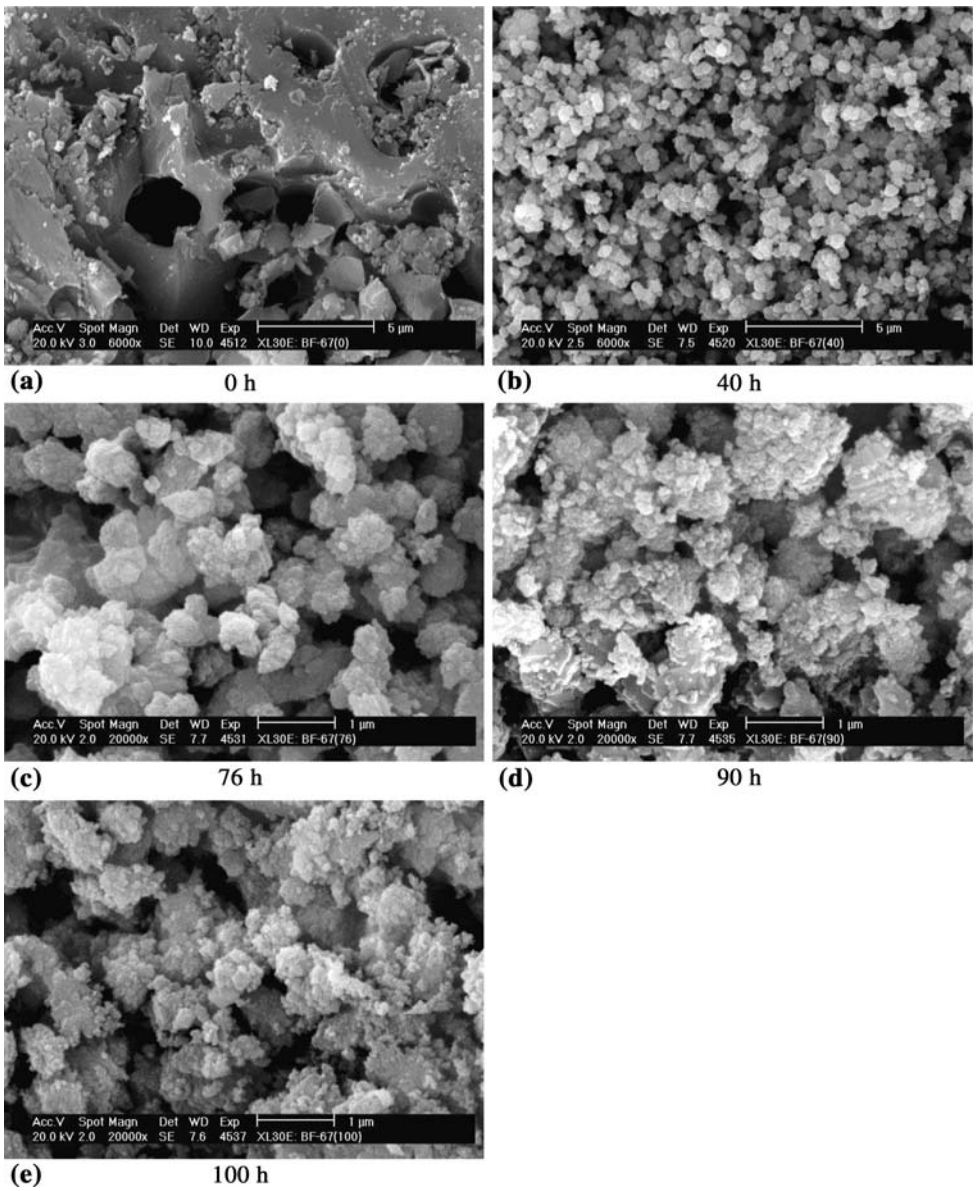

Fig. 2 The SEM of samples obtained during the crystallization process

in sample of crystallization time of 90 h. The size of the mordenite with acicular, cuboid or prismatic crystals was usually very large no matter if adding fluoride in initial reaction mixture [27–29]. Similar to STF/SFF intergrowth [17], the samples with high mordenite phase content were obtained while crystallization time was more than 82 h. The samples had homogeneity of crystal shape and there was no evidence to show the existence of pure mordenite.

Chemical composition of the samples

Chemical compositions of the samples with different crystallization time were displayed in Table 1. The initial amorphous gel has the relative high silica and sodium contents. At crystallization time 20 or 40 h, zeolite beta as the only solid product has a constant SAR (silica alumina ratio) for the effect of fluoride anions [30]. According to the liquid–liquid phase transformation mechanism, the high temperature resulted in the decreased induction period and the transition complex formed easily. During crystallization for 50–76 h period, the mordenite phase content was enhanced gradually as the crystallization time increased. Lower mordenite content in co-crystalline zeolite did not brought obvious influence on SAR of samples, which was basically maintained invariable in this period. When crystallization time exceed 76 h, the SARs of co-crystalline zeolite samples showed increase from about 21 to 24, which might result from the increased mordenite phase content with the increase of crystallization time. The increasing SARs of co-crystalline zeolite indicated that the

Table 1 The chemical composition of samples obtained at the different crystallization time (silica alumina molar ratio of gel is 25)

Crystallization time (h)	SAR*	Na contents (%)
0	27.2	4.83
20	21.2	0.63
40	21.3	0.38
50	20.7	0.39
62	20.9	0.34
76	21.2	0.36
82	24.1	0.40
90	23.7	0.91
100	24.0	0.96

* SAR = Silica alumina molar ratio

mordenite phase has the high SAR under dual structure directing action of organic amine ions and fluoride anions [21, 22].

Thermal analysis

The weight losses of obtained samples at different crystallization periods were shown in Table 2. The amorphous solid from initial gel has a large amount of physical adsorbed water. The weight losses corresponding to dehydration exceed 50% of total weight losses. In its DTG (differential thermal gravity analysis) curve (not shown herein), only a decomposition peak (at 280 °C) of TEA species occluded inside gel was observed except dewater peak. It indicated that the occluded TEA species in the initial gel were easily decomposed because the interaction between TEA and the gel was rather weak. After 20 h crystallization, both pure zeolite beta phase and amorphous aluminosilicate were presented. The DTG curve presented two well-pronounced mass loss peaks at 425 °C and 630 °C, which correspond to the decomposition of TEAOH and TEA cations interacting strongly with the framework containing Al species, respectively [31]. Similarly, after 40 h crystallization, with the amount of the amorphous aluminosilicate decreasing and the crystallinity of zeolite beta increasing, the peaks corresponding to the decomposition of TEAOH and TEA cations were increased to 435 °C and 638 °C, respectively. Furthermore, the content of total TEA species' in sample was increased simultaneously, which resulted in decrease of the concentration of TEA cations in the liquid phase. When crystallization time was further prolonged, the amount of TEA cations was not enough to produce the pure zeolite beta solely, so the mordenite phase appeared. When crystallization time was 50–62 h, the mordenite phase content in the co-crystalline zeolite was relatively lower. So the total mass loss amount in the different regions of TEA species did not have the distinct changes. While crystallization time exceeded 76 h, the SARs of co-crystalline zeolite increased gradually with crystallization time prolonging. Accordingly, the amount of TEA cations and TEAOH which plays the equalizing negative electric charges of framework Al and pore-filling role decreased.

Nitrogen adsorption–desorption isotherm

Nitrogen adsorption–desorption isotherm of initial gel showed type IVb adsorption isotherm behavior with a type H2 hysteresis loop [32, 33], which has a strong steep desorption branch and a more or less sloping adsorption branch (Fig. 3). H2 hysteresis loop indicated that there are highly disordered independent random pores with different size and shape in the sample. The amount of adsorbed nitrogen was lower. The total BET surface area was 103.6 m^2/g, but the micropore surface area was only 14.1 m^2/g.

The nitrogen adsorption–desorption isotherm curves of samples obtained at the different crystallization time were displayed in Fig. 4. The BET surface area, micropore surface area, and micropore volume data were listed in Table 3. All plots corresponded to type IIb adsorption isotherms with a type H3 hysteresis loop.

Table 2 The weight losses of samples obtained at the different crystallization time

Crystallization time (h)	Weight losses (%)					200–820 Total (%)
	0–200 °C	200–360 °C	360–500 °C	500–700 °C	700–820 °C	
0	10.3	7.0	2.1	0.7	0.5	10.2
20	3.1	2.3	7.8	4.6	0.1	14.8
40	1.3	2.0	8.5	5.1	0.1	15.6
50	2.2	1.9	8.7	4.5	0.1	15.2
62	2.9	1.7	8.7	4.8	0.1	15.3
76	2.6	1.7	8.5	4.3	0	14.4
82	3.5	1.5	8.0	4.1	0	13.4
90	2.7	1.4	7.0	3.0	0	11.3
100	2.6	1.3	6.8	2.9	0	11.0

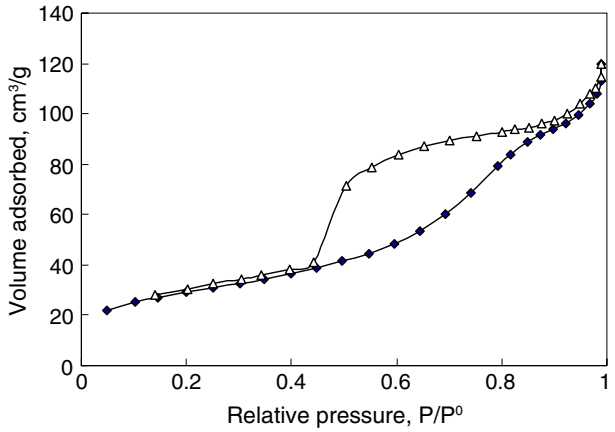

Fig. 3 Nitrogen adsorption–desorption isotherm of sample before crystallization

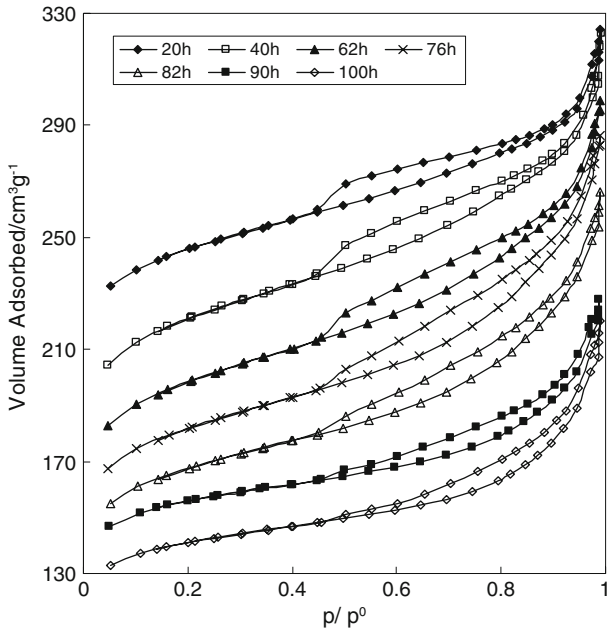

Fig. 4 The nitrogen adsorption–desorption isotherm curves of samples obtained at different crystallization time (Putting in 10 cm^3 g^{-1}offset for samples of 76, 90 h; 20 cm^3 g^{-1}offset for sample of 62 h; 40 cm^3 g^{-1}offset for sample 40 h; and 90 cm^3 g^{-1}offset for sample 20 h on the Y-axis)

The microporous zeolites usually exhibited type I adsorption isotherm. The presence of hysteresis loop, which appeared in the multilayer range of physisorption isotherms, was generally associated with the filling and emptying of mesopores. For two zeolite beta samples, the adsorbed nitrogen amount was ascended observably with the crystallinity increasing. It indicated that the relative crystallinity of two zeolite beta samples was not up to 100 %. With the crystallinity of pure zeolite increasing, the BET surface area, micropore surface area and micropore volume increased synchronously. However, the contributions to the specific surface area and pore volume of micropores were invariable.

Table 3 Determined value of BET surface area, micropore area and pore volume for various samples by nitrogen adsorption

Crystallization time (h)	Surface area (m^2 g^{-1})		Pore volume (cm^3 g^{-1})	
	BET	Micropore	Total	Micropore
0	104	14	0.185	0.01
20	504	346	0.363	0.172
40	585	404	0.438	0.200
62	578	404	0.432	0.200
76	556	395	0.428	0.195
82	539	393	0.412	0.195
90	468	372	0.337	0.184
100	452	361	0.341	0.178

Accompanied by increasing phase content of mordenite in intergrowth samples, the adsorbed nitrogen amount stepped down. Moreover, the BET surface area, micropore surface area and pore volume of samples decreased simultaneously though the variable extension of the micropore surface area was narrower than that of the BET surface area. In other words, formation of co-crystalline structure resulted in more influence on external surface, which could be attributed to their different framework structure character. Zeolite beta has three-dimensional structure, whereas mordenite has one-dimensional structure. The change of desorption branch at relative pressure P/P_0 of 0.45–0.5 should be noted. The discontinuity there became less pronounced with increased crystallization time and disappeared entirely with crystallization times exceeding 90 h. The hysteresis loop is associated with the filling and emptying of mesopores by capillary condensation. Isotherms with type H3 loops that do not level off at relative pressures close to the saturation vapor pressure were reported for materials composed of aggregates (loose assemblages) of platelike particles forming slit-like pores [32]. It indicated that the pore structure of co-crystalline samples, which possessed uneven pore distributions and was changed gradually, accompanied by the formation of the co-crystalline structure. In contrast, the adsorption–desorption isotherm of MOR/MFI core-shell type overgrowth was typical type I [19], which might be due to unitary microporous zeolite external surface.

The pore size distributions for the materials are shown in Fig. 5 derived from the desorption branch of the isotherms according to the BJH method. A single peak at 3.9 nm was observed in the pore size distribution curve for pure zeolite beta sample, which used to be considered as interparticle and uniform pores among molecular sieve granules. All samples exhibited sharp mesoporous peaks ranging from 3.2 to 4.4 nm, which tend to be gradually diminished with

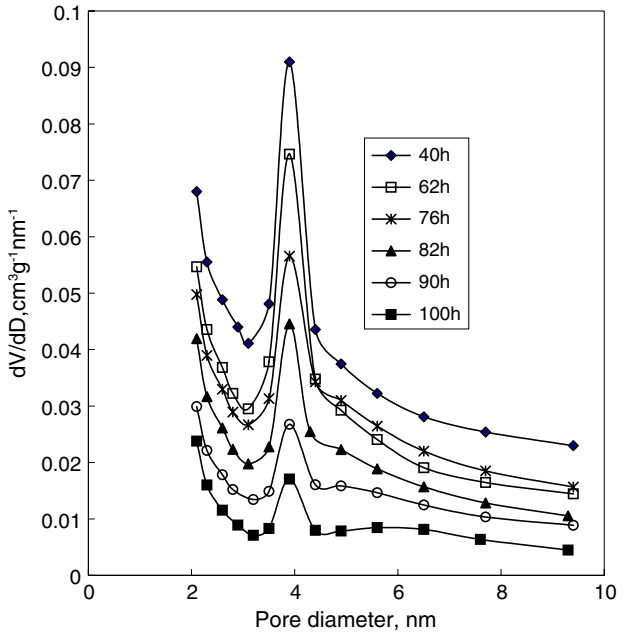

Fig. 5 Pore size distributions of samples obtained during the crystallization process (Putting in 0.02 cm^3 g^{-1} nm^{-1} offset for sample of 40 h; 0.01 cm^3 g^{-1} nm^{-1} offset for samples of 62 and 76 h; and 0.005 cm^3 g^{-1} nm^{-1} offset for samples of 82 and 90 h on the Y-axis)

the mordenite phase content in co-crystalline samples increasing. When crystallization time was elongated to 90 and 100 h, extra broad range of the mesoporous peaks which should be result from the production of BEA/MOR co-crystalline structure appeared and the pore sizes were 4.9 and 5.6 nm, respectively. The result of small-angle XRD for the sample obtained after 100 h crystallization (not shown here) excluded the possibility of the regular mesopores existing in BEA/MOR co-crystalline framework. So the extra mesopores maybe ascribed to other kinds of interparticle pores that are uneven slit-like pores with broad pore size distribution due to the asymmetric granularity distribution of the intergrowth particles. The special pore structure of BEA/MOR might be another reason for its high catalytic activity besides the specific acid character [1].

Crystallization process of BEA/MOR intergrowth

Based on the results reported above, an assumption about the crystallization mechanism of BEA/MOR composites is put forward as follows: At the beginning of crystallization process, zeolite beta with lower framework density is produced swiftly for the existence of the thermodynamic stability phase area giving rise to zeolite beta phase in synthesis system under the appropriate TEAOH content. Thereafter, as the crystallinity of zeolite beta increase, TEA species presented in the molecular sieve product are enhanced gradually and TEA cations in liquid phase are decreased accordingly. Both the gel and liquid phase compositions gradually changed. When TEA cations concentration in liquid phase was too low to satisfy the demand of synthesizing three-dimensional zeolite beta, the mordenite phase with higher framework density emerged. The thermodynamic stability phase area of crystallization system is shifted to produce BEA/MOR co-crystalline structure. Herein, zeolite beta particles produced earlier could correspond to the crystal seeds and direct the synthesis of BEA/MOR co-crystalline zeolite. The formation of mordenite phase in the composite predominates in this phase area. Due to the geometry factor, it is difficult for the granules of co-crystalline BEA/MOR to become big particles. Thus, slight change in morphology is exhibited during the crystallization process. The formation of the co-crystalline structure could be attributed to the alternative growth of zeolite beta and mordenite. Later in the crystallization, the crystallization rate of MOR phase was much faster than BEA phase. As the content of mordenite phase in BEA/MOR increased, the BET surface area, micropore surface area and pore volume of intergrowth decreased simultaneously. The asymmetry of BEA/MOR co-crystalline particles lead to the uneven mesopores distribution.

Conclusion

In the crystallization process of BEA/MOR co-crystalline zeolite, zeolite beta phase with the relative open framework structure formed first, and then another zeolite, mordenite phase with relative high framework density appeared. The morphology of particles obtained during the crystallization process changed a little, but the granularity distribution range broadened. The asymmetric BEA/MOR co-crystalline zeolite particles led to uneven mesopores distribution. When the crystallization time of the sample exceeded 90 h, bimodal mesopores were exhibited in pore size distribution curves of BEA/MOR intergrowth samples. An assumption about the crystallization mechanism of BEA/MOR was put forward, by which the phase content of intergrowth can be controlled by choosing appropriate crystallization time.

Acknowledgement This work was financially supported by the National Basic Research Program of China, grant No. 2003CB615802.

References

1. Qi X, Li B, Li S, Liu X, Lin B (2006) Chin J Catal 27:228
2. Niu X, Song Y, Xie S, Liu S, Wang Q, Xu L (2005) Catal Lett 103:211. doi:10.1007/s10562-005-7156-4
3. Gonzáleza G, Gonzáleza CS, Strackeb W, Reicheltb R, García L (2007) Microporous Mesoporous Mater 101:30. doi:10.1016/j.micromeso.2006.11.008

4. Francesconi MS, López ZE, Uzcátegui D, González G, Hernández JC, Uzcátegui A, Loaiza A, Imbert FE (2005) Catal Today 107–108:809. doi:10.1016/j.cattod.2005.07.013
5. Belandría LN, Días CSG, Hernández JC, Uzcátegui A, González G, Imbert F (2005) North American Catalysis Society 19th North American Meeting, May 2005, Philadelphia, p 262
6. Szostak R (1988) Molecular sieves principles of synthesis and identification, 2nd edn. Blackie Academic & Professional, London, p 62
7. Rao CNR, Thomas JM (1985) Acc Chem Res 18:113. doi:10.1021/ar00112a003
8. Gregory AJ, Sand LB, Gard JA (1986) Zeolites 6:396. doi:10.1016/0144-2449(86)90069-2
9. Goossens AM, Wouters BH, Buschmann V, Martens JA (1999) Adv Mater 11:561. doi:10.1002/(SICI)1521-4095(199905)11:7≤561::AID-ADMA561≥3.0.CO;2-Q
10. Goossens AM, Wouters BH, Grobet PJ, Buschmann V, Fiermans L, Martens JA (2001) Eur J Inorg Chem 2001:1167. doi:10.1002/1099-0682(200105)2001:5≤1167::AID-EJIC1167≥3.0.CO;2-Z
11. Hanif N, Anderson MW, Alfredsson V, Terasakic O (2000) Phys Chem Chem Phys 2:3349. doi:10.1039/b002314k
12. Leonowicz ME, Vaughan DEW (1987) Nature 329:819. doi:10.1038/329819a0
13. Jacobs PA, Martens JA (1987) Synthesis of high-silica aluminosilicate zeolites, studies in surface science and catalysis, vol 33, Elsevier Science, Amsterdam, p 342
14. Lillerud KP, Raeder JH (1986) Zeolites 6:474. doi:10.1016/0144-2449(86)90032-1
15. Yang S, Evmiridis NP (1996) Microporous Mater 6:19. doi:10.1016/0927-6513(95)00077-1
16. Liu X, Lin B, Qi X, Chen G (2003) CN patent 1397493
17. Villaescusa LA, Zhou W, Morris RE, Barrett PA (2004) J Mater Chem 14:1982. doi:10.1039/b315643e
18. http://www.iza-structure.org/databases/
19. Bouizi Y, Rouleau L, Valtchev VP (2006) Microporous Mesoporous Mater 91:70. doi:10.1016/j.micromeso.2005.11.016
20. Loos JB (1997) Zeolites 18:278. doi:10.1016/S0144-2449(97)00013-4
21. Qi X, Liu X, Wang Z (2001) Stud Surf Sci Catal 135:02P39
22. Qi X, Li S, Wang Z, Liu X, Lin B (2003) Chin J Catal 24:535
23. Qi X, Li S, Li B, Li N, Liu X, Lin B (2004) Chin J Catal 25:163
24. Qi X, Zheng J, Liu X (2006) In: Newman AM (ed) Focus on solid state chemistry, Nova Publishers, New York, p 95
25. Sasaki H, Oumi Y, Itabashi K, Lu B, Teranishi T, Sano T (2003) J Mater Chem 13:1173. doi:10.1039/b212519f
26. Fan W, Shirato S, Gao F, Ogura M, Okubo T (2006) Microporous Mesoporous Mater 89:227. doi:10.1016/j.micromeso.2005.11.001
27. Qi X, Wang Z, Li S, Li B, Liu X, Lin B (2006) Acta Phys-Chim Sin 22:198
28. Lu B, Tsuda T, Sasaki H, Oumi Y, Itabashi K, Teranishi T, Sano T (2004) Chem Mater 16:286. doi:10.1021/cm030576y
29. Shaikh AA, Joshi PN, Jacob NE, Shiralkar VP (1993) Zeolites 13:511. doi:10.1016/0144-2449(93)90227-T
30. Qi X, Liu X, Chen G, Lin B (2000) Chem J Chin Univ 21:1161
31. Kim DS, Chang JS, Hwang JS, Park SE, Kim JM (2004) Micropor Mesopor Mater 68:77. doi:10.1016/j.micromeso.2003.11.017
32. Kruk M, Jaroniec M (2001) Chem Mater 13:3169. doi:10.1021/cm0101069
33. Rouquerol J, Rouquerol F, Sing KSW (1999) Adsorption by powders and porous solids: principle, methodology and applications. Academic Press, London, p 440